Fall 9-15-2015

Applications and Comparison of Continuous Wavelets Transforms on Analysis of A-wave Impulse Noise

Jun Qin
Southern Illinois University Carbondale, jqin@siu.edu

Pengfei Sun
Southern Illinois University Carbondale, sunpengfei@siu.edu

Recommended Citation
Qin, Jun and Sun, Pengfei. "Applications and Comparison of Continuous Wavelets Transforms on Analysis of A-wave Impulse Noise." *Archives of Acoustics* 40, No. 4 (Fall 2015): 503-512. doi:10.1515/aoa-2015-0050.

PAN ARCHIVES OF ACOUSTICS
Vol. **40**, No. 4, pp. 503–512 (2015)

DOI: 10.1515/aoa-2015-0050

Applications and Comparison of Continuous Wavelet Transforms on Analysis of A-wave Impulse Noise

Jun QIN, Pengfei SUN

Department of Electrical and Computer Engineering
Southern Illinois University Carbondale
1230 Lincoln Drive, Mail Code 6603, Carbondale, IL 62901, USA; e-mail: jqin@siu.edu

(*received August 19, 2014; accepted September 25, 2015*)

Noise induced hearing loss (NIHL) is a serious occupational related health problem worldwide. The A-wave impulse noise could cause severe hearing loss, and characteristics of such kind of impulse noise in the joint time-frequency (T-F) domain are critical for evaluation of auditory hazard level. This study focuses on the analysis of A-wave impulse noise in the T-F domain using continual wavelet transforms. Three different wavelets, referring to Morlet, Mexican hat, and Meyer wavelets, were investigated and compared based on theoretical analysis and applications to experimental generated A-wave impulse noise signals. The underlying theory of continuous wavelet transform was given and the temporal and spectral resolutions were theoretically analyzed. The main results showed that the Mexican hat wavelet demonstrated significant advantages over the Morlet and Meyer wavelets for the characterization and analysis of the A-wave impulse noise. The results of this study provide useful information for applying wavelet transform on signal processing of the A-wave impulse noise.

Keywords: continuous wavelet transform, impulse noise signal processing, time-frequency domain, temporal and spectral resolutions, noise induced hearing loss, A-wave impulse noise.

1. Introduction

Noise induced hearing loss (NIHL) is a serious problem that affects many people worldwide. According to the World Health Organization, exposure to excessive noise is the major avoidable cause of permanent hearing loss (Smith, 1996). It is estimated that about 29 million Americans have some type of hearing loss within the speech frequency range (Agrawal *et al.*, 2008). A-wave impulse noise is a type of highly transient noise widely experienced in military fields (e.g., an intense blast wave) (Henderson, Hamernik, 1986). A typical waveform of A-wave impulse noise is illustrated in Fig. 1. It is leading by a sharp compressive wave with time duration (referred as A-duration) about 0.5 ms, and followed by a tensile wave of about 1 ms duration (Henderson, Hamernik, 1986). Animal studies demonstrated that the impulse noise could cause more hearing loss than continuous Gaussian noise with same amount of acoustic energy (Hamernik *et al.*, 1993).

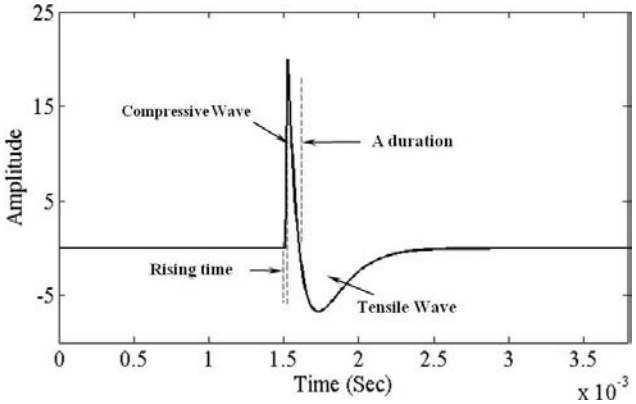

Fig. 1. A schematic representation of a typical A-wave impulse noise.

Characteristics of the impulse noise in both time and frequency domains are critical for evaluation of auditory hazard level and prediction of NIHL (Price *et al.*, 1989). The fast Fourier transform (FFT) has been widely used to analyze and display the spectrum of noise signals in the frequency domain (Clifford, Rogers, 2009). However, the FFT only provides the time history or the frequency spectrum alone, and they are not sufficient to analyze transient signals (e.g., im-

pulse noise). In addition, the short-time Fourier transform (STFT) has also been used to analyze transient signals, and it can provide detailed information in the joint time-frequency (T-F) domain. However, because of fixed time window, STFT could lose the spectral resolution in low frequency range, while it also could lose the temporal resolution in high frequency range (Zhu, Kim, 2006).

In contrast, the wavelet transform (WT) uses wavelet function and various scales to decompose signals in the T-F domain, and it can guarantee the temporal and spectral resolutions in the entire frequency range. Since introduced in the 1970s, WT has been used in various applications, such as signal detection, imaging processing, signal de-noising, speed enhancement, audio classification, etc. (Mallat, 1997). Wang and colleagues applied the Morlet WT for mechanical fault diagnosis. They extracted features of the impulse signals on both time and frequency domains. Based on the T-F localization, the wavelet coefficients were investigated to classify the acoustic signals, and to recognize the faults of mechanical structure (Wang, McFadden, 1996; Lin, Qu, 2000). Satish and Nazneen used WT as an effective tool to obtain the partial discharge signals buried in excessive noise and interferences (Satish, Nazneen, 2003). Adeli *et al.*, developed a WT based algorithm for characterization of the spike of epileptic form discharges, and based on the wavelet decomposition of the electroencephalogram records, the captured transient features were investigated to reveal the small-scale oscillations (Senhadji, Wendling, 2002; Adeli *et al.*, 2003).

In addition, WT has also been used for noise analysis. Zhu and Kim applied the analytic wavelet transform to analyze the impact noise and vibrations (Zhu, Kim, 2006; Kim *et al.*, 2007). The Morlet wavelet was used in their study, in which the parameters were improved based on 1/3 octave bands in the frequency range. Their results demonstrated that the WT could capture much more detailed characteristics of transient signals than the STFT (Zhu, Kim, 2006).

However, the application of WT to the A-wave impulse noise has not been investigated. In this paper, we will apply the continuous wavelet transform to analyze the A-wave impulse noise signals generated by a noise exposure system, which was developed to mimic A-wave impulse noise produced by a military weapon (e.g., M-16 rifle) (Wu, Qin, 2013). Three different wavelets, including the Morlet, Mexican hat, and Meyer wavelets, were investigated and compared based on theoretical analysis and applications to experimental generated A-wave impulse noise signals. The underlying theory of continuous wavelet transform was given and the temporal and spectral resolutions were theoretically analyzed. The wavelet entropy and the similarity between the wavelets functions and the noise signal were investigated and discussed in this paper as well.

2. Underlying theory and theoretical analysis

2.1. General theory of CWT

Continuous wavelet transform (CWT) which decomposes a signal $f(t)$ in the T-F domain can be defined as follows (Daubechies, 1992; Mallat, 1997):

$$W(a,b) = \int_{-\infty}^{\infty} f(t)\frac{1}{\sqrt{a}}\psi\left(\frac{t-b}{a}\right)\,\mathrm{d}t, \tag{1}$$

where $\psi(t)$ is the wavelet kernel function along with the continuous scaling parameter a and the time shifting parameter b. $W(a,b)$ refers to the CWT coefficient.

The signal $f(t)$ can be recovered back from the CWT coefficients only when it satisfies the admissibility condition ($C_\psi < \infty$):

$$f(t) = C_\psi^{-1}\int_{-\infty}^{\infty}\int_{0}^{+\infty}\frac{\mathrm{d}a\,\mathrm{d}b}{a^2}W(a,b)\psi(t), \tag{2}$$

where constant value C_ψ is defined by:

$$C_\psi = 2\pi\int_{-\infty}^{\infty}\mathrm{d}\omega\left|\widehat{\psi}(\omega)\right|^2|\omega|^{-1}, \tag{3}$$

where $\widehat{\psi}(\omega)$ is the Fourier transform of the wavelet kernel function $\psi(t)$. Equation (3) requires that $\widehat{\psi}(0) = 0$, which equals to $\int\psi(t)\,\mathrm{d}t = 0$, and wavelet kernel functions have a zero average in the time domain (Mallat, 1997). In addition, after normalization, $\int|\psi(t)|^2\,\mathrm{d}t = 1$ is required as well.

2.2. Three different continuous wavelets

In this paper, three continuous wavelets, Morlet, Mexican hat and Meyer wavelets, are investigated. The Morlet wavelet is derived from the Gaussian function, while the Mexican hat wavelet is defined according to the second derivative of Gaussian function. In addition, the Meyer wavelet is an orthogonal wavelet, and it is defined on the frequency domain. Typically, the kernel functions of three wavelets, $\psi_{\mathrm{morl}}(t)$, $\psi_{\mathrm{mexh}}(t)$, and $\psi_{\mathrm{meyr}}(t)$, can be described by the following equations, respectively (Mallat, 1997).

$$\psi_{\mathrm{morl}}(t) = \frac{1}{\sqrt{\pi f_b}}e^{-t^2/f_b}e^{2i\pi f_c t}, \tag{4}$$

$$\psi_{\mathrm{mexh}}(t) = \frac{2}{\sqrt{3\sigma}\pi^{1/4}}\left(1-\frac{t^2}{\sigma^2}\right)e^{-t^2/2\sigma^2}, \tag{5}$$

$$\psi_{\mathrm{meyr}}(t) = \int_0^{\infty}\sin[\lambda(\omega)]\cos\left[\left(t-\frac{1}{2}\right)\omega\right]\mathrm{d}\omega, \tag{6}$$

where f_b, f_c in Eq. (4) are the bandwidth parameter and center frequency, respectively. In this study, the real part of Eq. (4) will be used to represent Morlet wavelets. σ in Eq. (5) is constant parameter. λ in Eq. (6) is an even function of ω.

To normalize wavelet kernel function $\psi(t)$, a wavelet atom $\phi_\gamma(t)$ is proposed:

$$\phi_\gamma(t) = \psi_{a,b}(t) = \frac{1}{\sqrt{a}}\psi\left(\frac{t-b}{a}\right), \tag{7}$$

where γ is a multi-index parameter referring to a and b.

Figure 2 shows the time history and frequency spectrum of the wavelet kernel functions of three wavelets. All three wavelets are symmetric about y-axis in the time domain. In the frequency domain, all three wavelets behave like band-pass filters, and they can extract the localized frequency details of transient signals. The bandwidth of the Mexican hat wavelet is narrower than the corresponding values of the other two wavelets.

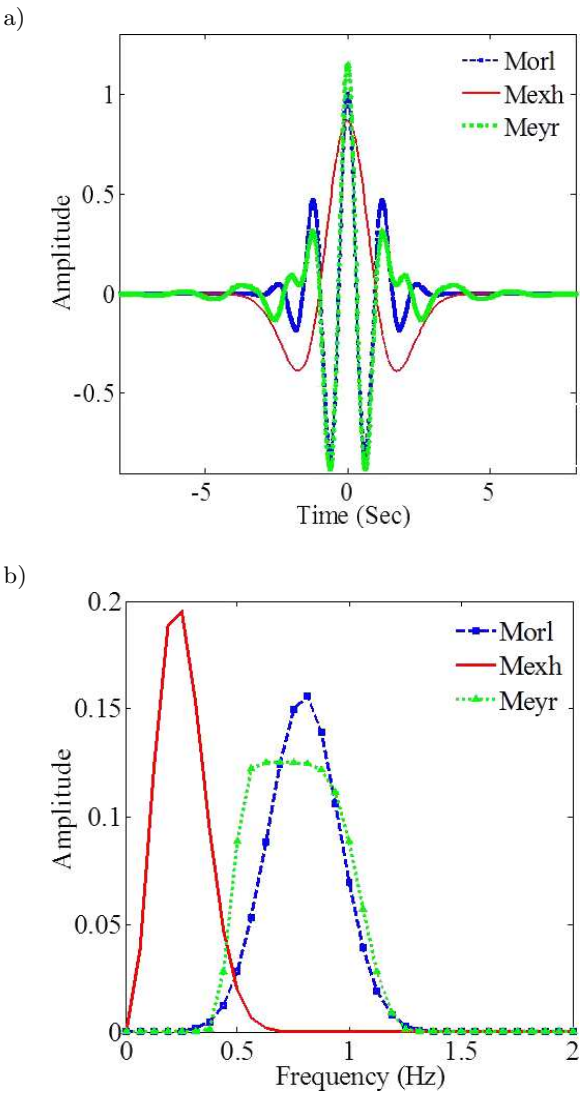

Fig. 2. a) Time history and b) frequency spectrum of wavelet kernel functions of the Morlet (Morl), Mexican hat (Mexh), and Meyer (Meyr) wavelets.

2.3. Temporal and spectral resolutions in the CWT.

Resolutions in the time and frequency domains are critical for evaluation of performance of different wavelets. The temporal resolution in the time domain σ_t and the spectral resolution in the frequency domain σ_ω of CWT can be defined as (Mallat, 1997):

$$\sigma_t^2(\gamma) = \int_{-\infty}^{+\infty} (t-u_\gamma)^2 \left|\phi_\gamma(t)\right|^2 \mathrm{d}t, \tag{8}$$

$$\sigma_\omega^2(\gamma) = \frac{1}{2\pi}\int_{-\infty}^{+\infty} (\omega-\xi_\gamma)^2 \left|\widehat{\phi}_\gamma(\omega)\right|^2 \mathrm{d}\omega, \tag{9}$$

where

$$u_\gamma = \frac{1}{\|\phi_\gamma\|^2}\int_{-\infty}^{+\infty} t\left|\phi_\gamma(t)\right|^2 \mathrm{d}t,$$

$$\xi_\gamma = \frac{1}{2\pi\|\phi_\gamma\|^2}\int_{-\infty}^{+\infty} \omega\left|\widehat{\phi}_\gamma(\omega)\right|^2 \mathrm{d}\omega,$$

$$\|\phi_\gamma\|^2 = 1,$$

and $\widehat{\phi}_\Upsilon(\omega)$ is the Fourier transform of the wavelet atom $\phi_\gamma(t)$.

Figures 3a and 3b show the theoretical analysis of temporal and spectral resolutions of three different wavelets with the scale a changing. For all three wavelets, the temporal resolutions decrease with the scale increasing (Fig. 3a), while the spectral resolutions increase with the scale increasing (Fig. 3b). To analyze a highly transient signal, such as an impulse noise signal, its short time duration requires small scales with high temporal resolution. When the scales become small, the temporal resolution of three wavelets are same (Fig. 3a). However, the Mexican hat wavelet shows the better spectral resolution than the Morlet and Meyer wavelets at small scales (Fig. 3b). Therefore, the Mexican hat wavelet has obvious advantages of better spectral resolution compared with the other two wavelets when applied to highly transient signal (e.g., impulse noise).

In addition, the resolution cell can be defined as the product of the temporal and spectral resolutions, and it is dynamically limited by $1/4\pi$, known as uncertainty principle (i.e., $\sigma_t \cdot \sigma_\omega \geq 1/4\pi$) (Young, 1993). As shown in Fig. 3c, the resolution cells of three different wavelets are constant with the scale increasing. The resolution cells of the Mexican hat ($[\sigma_t \cdot \sigma_\omega]_{\mathrm{mexh}} = 0.0836$) and the Morlet wavelets ($[\sigma_t \cdot \sigma_\omega]_{\mathrm{mol}} = 0.0796$), are comparable, and they are smaller than the corresponding value of the Meyer wavelet ($[\sigma_t \cdot \sigma_\omega]_{\mathrm{meyr}} = 0.1058$).

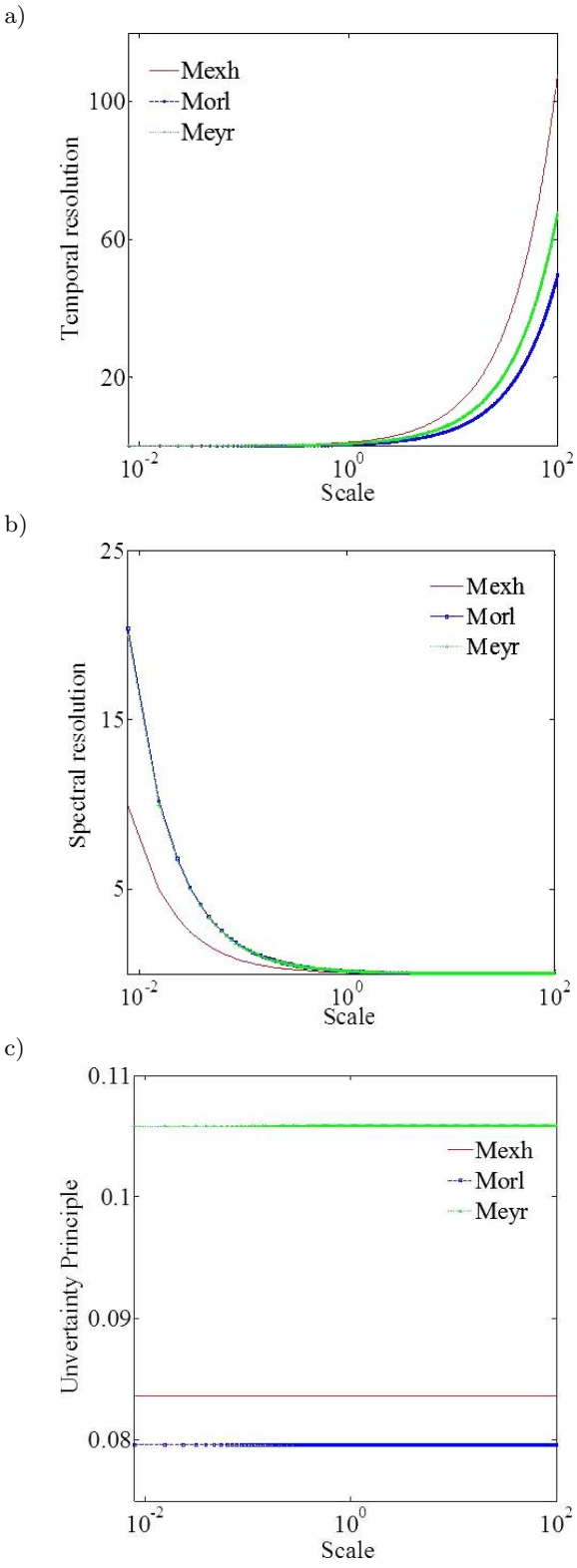

Fig. 3. a) Temporal resolution σ_t, b) spectral resolution σ_f, and c) resolution cell $(\sigma_t \cdot \sigma_f)$ of three different wavelets.

2.4. Wavelet entropy

The wavelet entropy reflects the energy cost of CWT. It has been used to evaluate the performance of CWT and to select the best wavelet kernel function. In general, the lower wavelet entropy indicates the better performance of CWT (Coifman, Wickerhauser, 1992).

The WT coefficients $W(a,b)$ represent the energy distribution of a signal in the T-F domain. The energy component E_a at each scale level a can be calculated by the WT coefficient as:

$$E_a = \sum_b |W(a,b)|^2 . \tag{10}$$

Consequentially, the total energy E_t of a CWT can be obtained by

$$E_t = \sum_a E_a. \tag{11}$$

Relative wavelet energy p_a can be defined as (Rosso *et al.*, 2001):

$$p_a = \frac{E_a}{E_t}. \tag{12}$$

Further, wavelet entropy S can be defined as

$$S = -\sum_a p_a \cdot \mathrm{In}(p_a). \tag{13}$$

In this study, the relative wavelet energy p_a and wavelet entropy S of three different wavelets will be calculated and compared.

2.5. Similarity analysis between wavelet functions and the waveform of impulse noise

When wavelet functions are similar to the original signal, CWT can accurately represent the original signal in the T-F domain. The similarity between the original signal and the wavelet functions can be used to evaluate the performance of CWT. The similarity can be defined as the error function $E(\psi(t),a)$ (Chapa, Rao, 2000):

$$E(\psi(t),a) = \int_{t_1}^{t_2} \left(f(t) - \frac{1}{\sqrt{a}} \psi\left(\frac{t}{a}\right) \right)^2 \mathrm{d}t, \tag{14}$$

where $f(t)$ refers to the original signal, $\psi(t)$ is the wavelet kernel function, and a is scale.

The error function inversely presents the similarity. On other words, when the coefficient of the error function reaches the minimal value, the wavelet function has the highest similarity to the original signal.

3. Experimental methods

3.1. Generation and measurement of impulse noise signals

The impulse noise signals used in this paper were generated by a digital noise exposure system, which

was developed in our lab to mimic the A-wave impulse noise produced by a military weapon (e.g., M-16 rifle) (Wu, Qin, 2013). As shown in Fig. 4a, the noise exposure system consists of a data acquisition device (DAQUSB-6251, Nation Instrument Inc., TX, USA), an audio power amplifier, an acoustic compression driver (2446H, JBL Professional, CA, USA), a shock tube extension, a flat-front horn (2380A, JBL Professional, CA, USA), and a computer. To mimic the impulse noise in military fields, the waveform of the digital signal can be described by the Friedlander wave:

$$p(t) = P_s e^{t/t^*}\left(1 - \frac{t}{t^*}\right), \tag{15}$$

where P_s is the peak sound pressure, and the t^* is the time at which the pressure crosses the x-axis and goes from positive to negative.

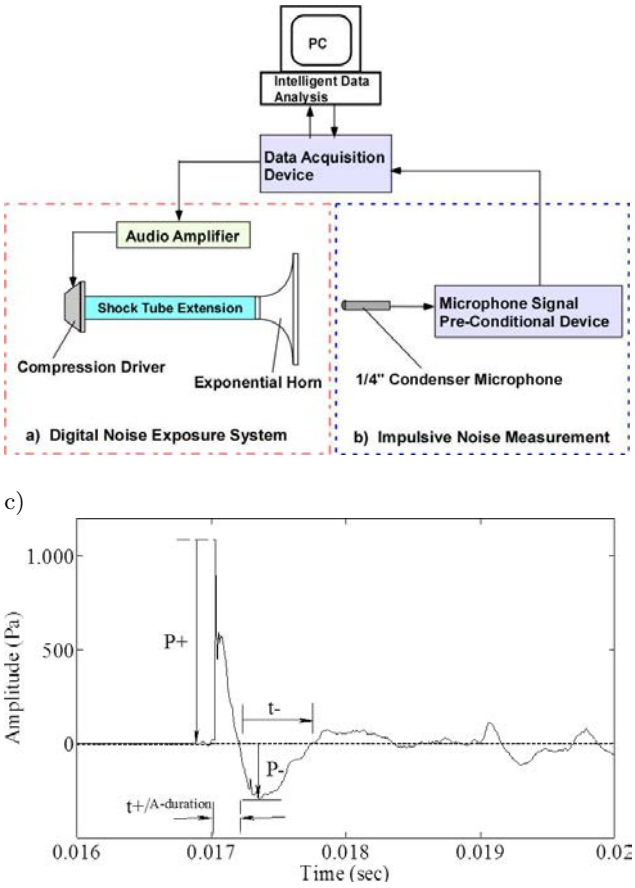

Fig. 4. Schematic diagram of the a) digital noise exposure system and b) impulse noise measurement system, and c) a representative waveform of A-wave impulse noise with peak SPL = 155 dB generated by the system.

The digital signals of impulse noise were generated based on Eq. (15) in LabVIEW, and then converted into analog signals through the data acquisition device with 131 kHz sampling rate. The analog signals were amplified by the audio power amplifier, and fed into the compression driver to create impulse noise.

A $1/4''$ condenser microphone set (46BE, G.R.A.S., Denmark) was used to measure the impulse noise (as shown in Fig. 4b). The sampling rate used in noise generation and measurement was 131 kHz. The impulse noise generated at different output voltage levels were measured, and 10 signals were saved at each voltage level. A typical waveform of A-wave impulse noise generated by the system is shown in Fig. 4c. The peak sound pressure level (SPL) is about 155 dB and the A-duration is about 0.5 ms.

3.2. Numerical implementation of CWT

Because all the three wavelets are symmetric functions, Eq. (1) can be written as a convolution integral form:

$$W(a,b) = \int_{-\infty}^{\infty} f(t)\frac{1}{\sqrt{a}}\psi\left(\frac{b-t}{a}\right)\mathrm{d}t = conv(f(t)\phi_\gamma(t)). \tag{16}$$

Further, the wavelet kernel functions are assumed to satisfy the admissibility condition in Eq. (3). Using the convolution property of Fourier transform, the Fourier transform of WT coefficients can be calculated as:

$$\widehat{W}(a,\omega) = \widehat{f}(\omega)\widehat{\phi_\gamma}(\omega), \tag{17}$$

where $\widehat{f}(\omega)$ and $\widehat{\phi_\gamma}(\omega)$ are the Fourier transforms of $f(t)$ and $\phi_\gamma(t)$. Therefore, the WT coefficients can be calculated by the inverse Fourier transform of $\widehat{W}(a,\omega)$. Based on the numerical method, the angular frequency ω can be defined as:

$$\omega = \omega_c/(a \cdot \Delta t), \tag{18}$$

where ω_c is the center frequency of kernel wavelet function, and Δt refers to the time interval.

3.3. Optimization of scales

To avoid the redundant decomposition of impulse noise, it is critical to optimize the scales in CWT. The optimization of scales can accurately extract significant features in the T-F domain, and save the computation resources as well. In an impulse noise, the local transient details require the higher scale density to illustrate the temporal and spectral information. The optimization of scales in this study is approached through the following steps (as shown in Fig. 5):

1. Set the upper value S_{upper} and the lower value S_{lower} for the scale;
2. Select a set of sorted scales $S_{\{i\}}$, and then calculate WT coefficient $W_{\{i\}}$;
3. Search $S_{\{j\}}$ where the WT coefficient $W_{\{i\}}$ reach local maximum or minimum value, and obtain j;

4. Decrease scale step $\Delta S_{\{j\}}$ to $\Delta S_{\{j\}}/2$. Based on new step value, add new scale into $S_{\{j\}}$, and then obtain $S_{\{j\}'}$ and $\{j\}'$. Calculate new WT coefficient $W_{\{j\}'}$;
5. $\forall n \in \{j\}$, if $(W_{\{n\}'} - W_{\{n\}})/W_{\{n\}} < \mu$, $\{j\} = \{j\} - n$, and $S_{\{i\}} = S_{\{i\}} + S_{\{n\}'}$; if $\{j\} \neq \{\emptyset\}$, repeat step (4);
6. Output the optimal scales $S_{\{i\}}$ and the WT coefficient.

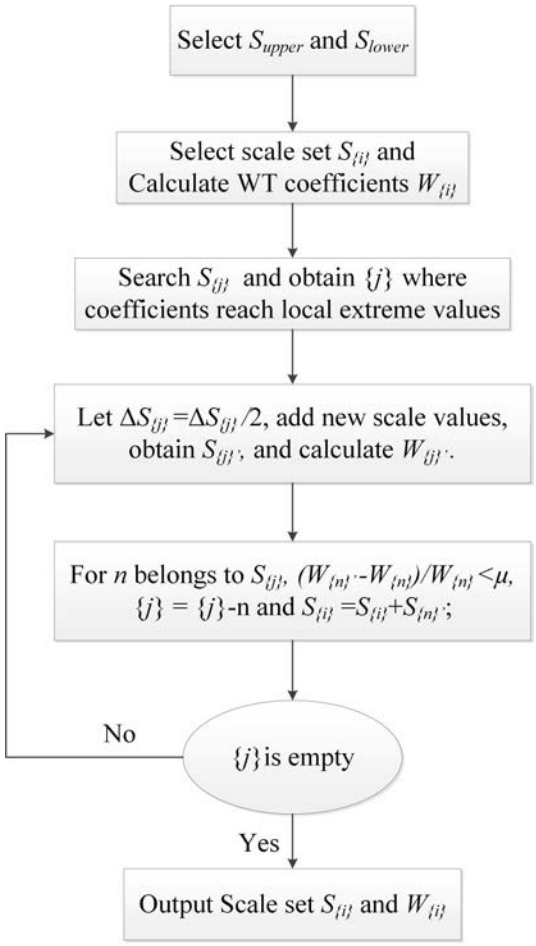

Fig. 5. Block diagram of the optimization of the scale a in the CWT.

4. Results and discussions

4.1. T-F characterization of impulse noise

Figure 6a shows the T-F representations obtained by applying the CWTs to a representative impulse noise signal (as shown in Fig. 4c) using the Morlet, Mexican hat and Meyer wavelets. All three wavelets can decompose the impulse noise and display detailed features in the T-F domain. Along the frequency axis, the spectrum distribution of three wavelets show similar trend. The amplitudes increase first and then decrease with the frequency increasing, and the peak

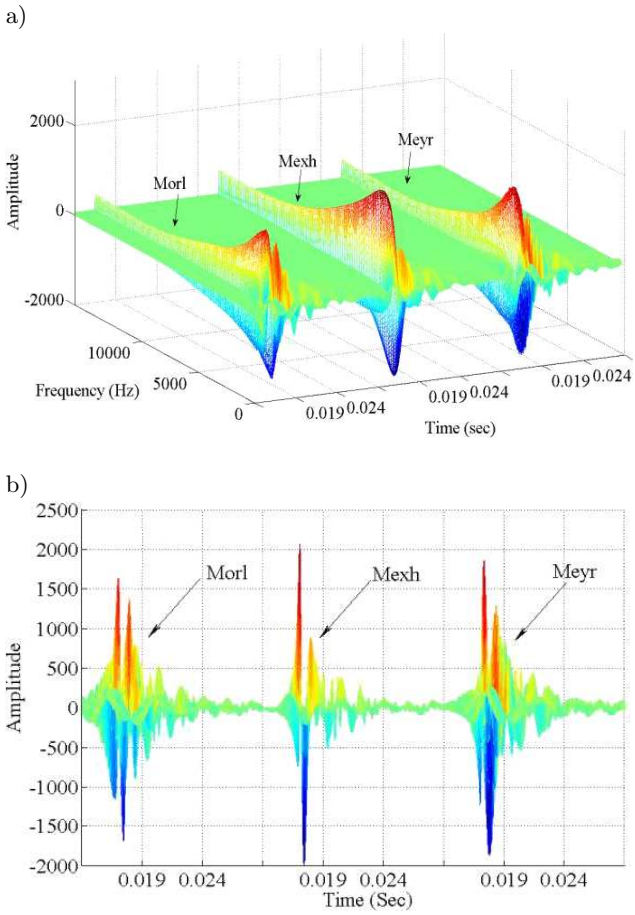

Fig. 6. a) time-frequency joint representations and b) distribution along the time axis obtained by applying the CWTs to a representative impulse noise signal using Morlet, Mexican hat and Meyer wavelets.

amplitudes can be found at frequency about 2000 Hz. The Mexican hat wavelet shows the highest peak amplitude among three wavelets. Along the time axis, all three wavelets cannot exactly represent the original signal of impulse noise (as shown in Fig. 6b). The Mexican hat wavelet shows the highest similarity to the original signal with less distortion compared with the Morlet and Meyer wavelets.

Figure 7 shows the time histories at five selected frequancies (i.e., 1 kHz, 2 kHz, 3 kHz, 4 kHz, and 5 kHz) of the CWTs using three wavelets. At all five frequences, the time histories produced by the Morlet and Meyer wavelets show more oscillation and signal distortion than the Mexican hat wavelet. In other words, the time histories produced by the Mexican hat wavelet show the highest similarity with the original signal. In addition, at high frequencies (3, 4, and 5 kHz), the amplitudes of the Mexican hat wavelet are higher than the corresponding values of the other two wavelets. It indicates that the Mexican hat wavelet has higher power spectrum and can provide more details than other two wavelets in high frequency range.

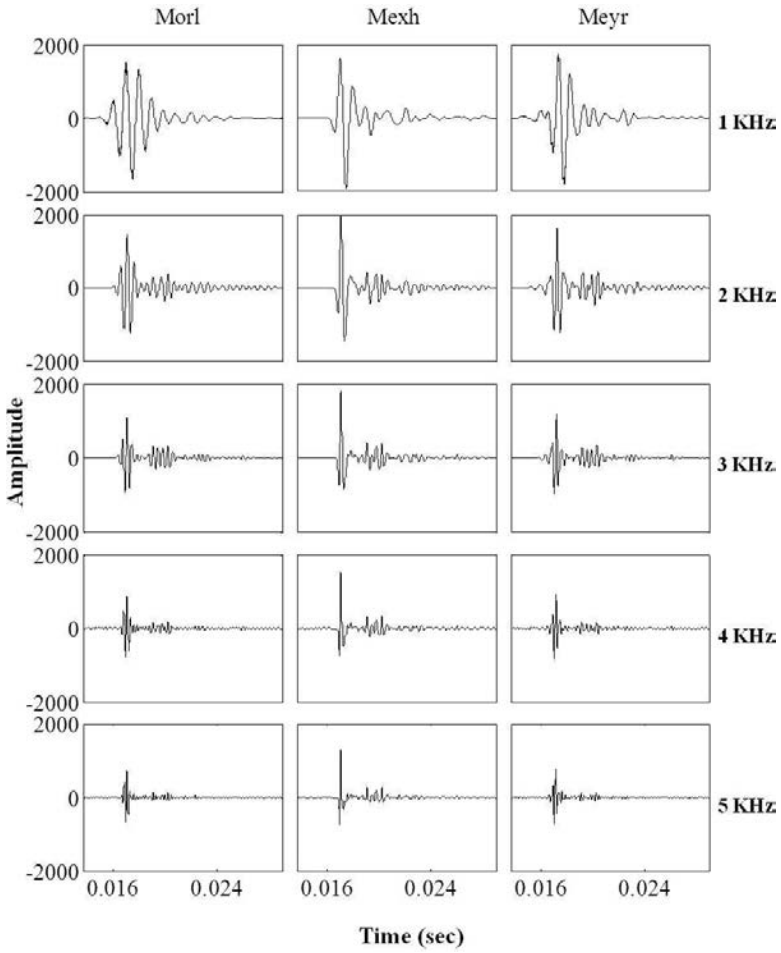

Fig. 7. Time histories at five selected frequancies (i.e., 1 kHz, 2 kHz, 3 kHz, 4 kHz, and 5 kHz) of the CWTs using three different wavelets.

4.2. Detection of singularity of the impulse noise signal in CWT

CWT is often applied to detect the singularities of a transient signal. The term 'ridge' was used to indicate the local transient values in CWT, and it represents related singular points in the original signal (Mallat, 1997). Figure 7 shows detection of the singularities in impulse noise signal in the color illustrated T-F domain using three different wavelets. The ridges can be determined by different neighboring colors in Fig. 8.

Figures 8b, 8c, and 8d illustrate the CWTs of impulse noise signal using the Morlet, Mexican hat, and Meyer wavelets, respectively. The numbers of ridges can be found to be 7 of the Morlet wavelet, 4 of the Mexican hat wavelet, and 7 of the Meyer wavelet. In addition, as illustrated in Fig. 8a, four singular points can be found in the original signal of impulse noise. The results show that the Mexican hat wavelet can accurately detect the singularities in the impulse noise signal. The Morlet and Meyer wavelets both have certain extent deviation on the singularity detection.

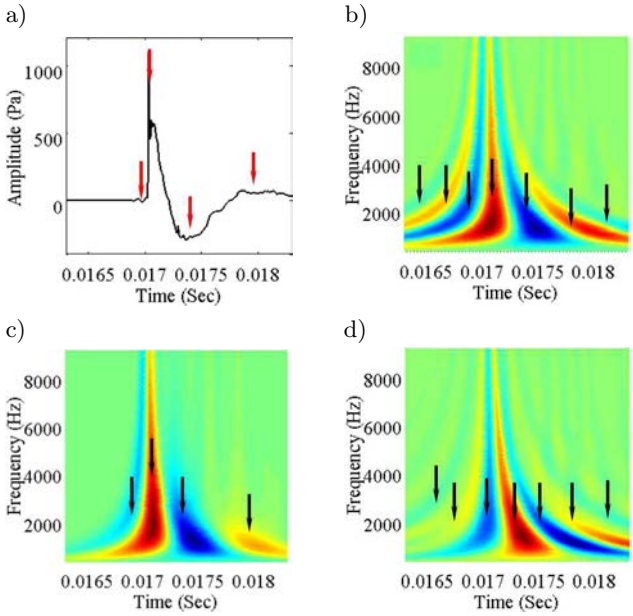

Fig. 8. a) A representative waveform of the impulse noise, and the color illustrated T-F representations of the impulse noise using the b) Morlet, c) Mexican hat, and d) Meyer wavelets.

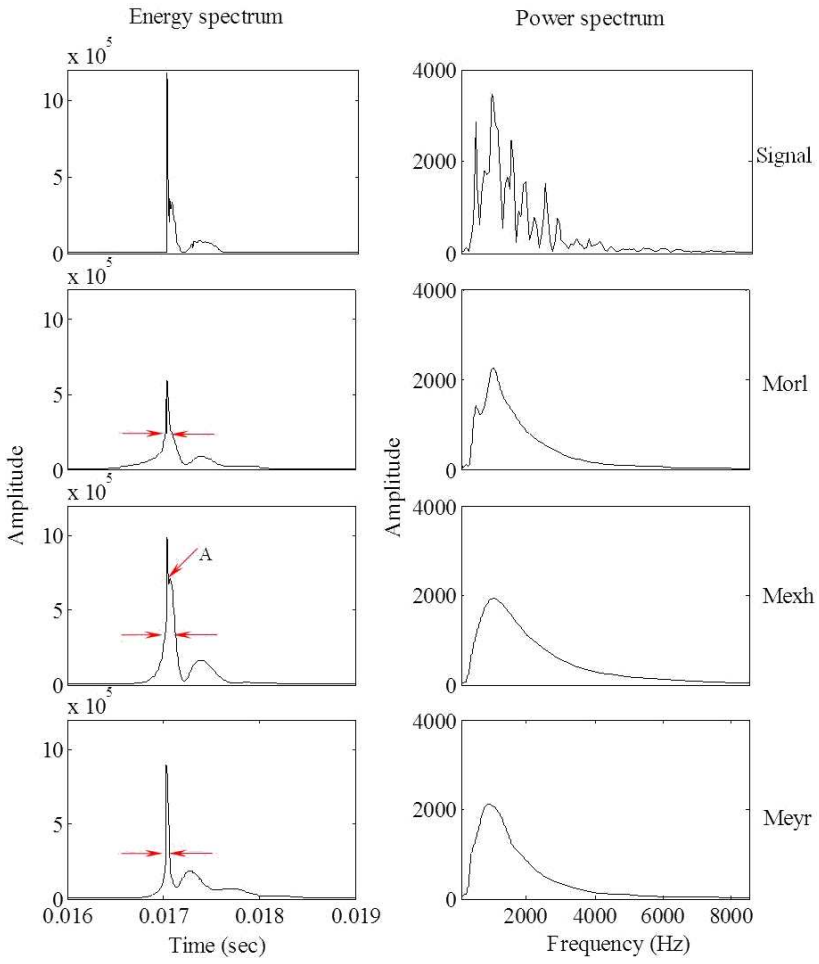

Fig. 9. The energy spectrum and power spectrum calculated using the original signal of impulse noise, and the WT coefficient produced by three different wavelets.

4.3. Energy spectrum and power spectrum

To further evaluate three wavelets, the energy spectrum and power spectrum of CWTs are calculated and compared with the corresponding values of the original impulse noise signal. The energy spectrum $E(t)$ and power spectrum $P(\omega)$ of the WT coefficient $W(t,\omega)$ are defined as:

$$P(\omega) = \int |W(t,\omega)|^2 \, \mathrm{d}t, \tag{19}$$

$$E(t) = \int |W(t,\omega)|^2 \, \mathrm{d}\omega. \tag{20}$$

Figure 9 illustrates the energy spectrum and power spectrum calculated using the original signal of impulse noise and the WT coefficient produced by three different wavelets, respectively. The left figures display the energy spectrums in the time domain. The Mexican hat wavelet produced higher energy spectrum than the Morlet and Meyer wavelets. In addition, the distribution of the energy spectrum of the Mexican hat wavelet is comparable to the original signal (as shown in the top left figure). The Mexican hat wavelet can represent transition points in the original signal such as the point A illustrated in Fig. 9c. It is because the Mexican hat wavelet has higher spectral resolution than the other two wavelets. This is consistent with the results of singularity detection.

The right figures in Fig. 9 show the power spectrum in the frequency domain. There is no significant difference among the power spectrums produced by three different wavelets. Moreover, all the power spectrums of three wavelets are comparable with it of the original signal by applying the regular FFT (as shown in the top right figure).

4.4. Relative wavelet energy and wavelet entropy

Figure 10a shows the distribution of relative wavelet energy of three wavelets with the scales changing. The relative energy of the Mexican hat wavelet is concentrated in a narrow scale range ($0 < a < 100$), while the relative energy of the Morlet and Meyer

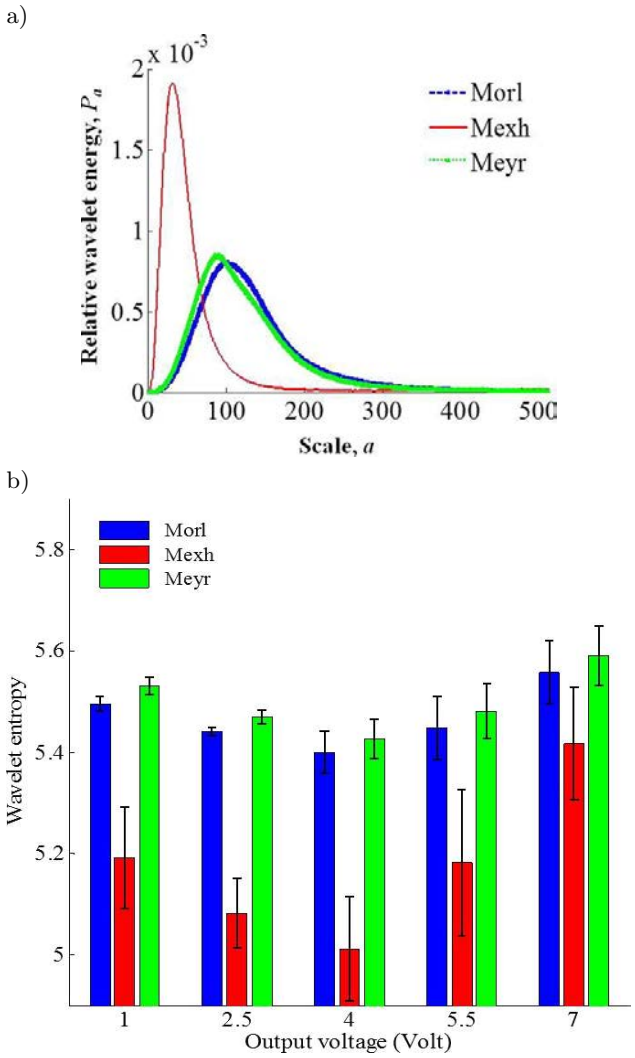

Fig. 10. a) Distribution of relative wavelet energies with scales increasing and b) wavelet entropies of the impulse noise signals generated at five varied output voltages by applying CWTs using three different wavelets.

wavelets are distributed in a broad scale range ($0 < a < 300$). In addition, the peak energy of the Mexican hat wavelet is about three times higher than it of the other two wavelets. The results indicate that the Mexican hat wavelet has higher degree of energy concentration on signal decomposition and it can represent detailed features (e.g., transient points) of the impulse noise signals with fewer scales.

Figure 10b shows the wavelet entropies of CWTs applied to the impulse noise using three different wavelets. The signals of impulse noise were generated by the developed noise exposure system (as shown in Fig. 4a) at five output voltages (i.e., 1.0, 2.5, 4.0, 5.5 and 7.0 V). Ten signals at each output voltages were measured and used to calculate the wavelet entropies of CWTs. At all five output voltages, the Mexican hat wavelet show significantly lower wavelet entropy than the other two wavelets. The results indicate that the Mexican hat wavelet requires lower information cost when decomposing the impulse noise signal compared with the other two wavelets.

4.5. Similarity analysis

Figure 11 shows the similarities between the impulse noise signal and three different wavelets under different scales. When the scale is less than 40, which is corresponding to the frequency higher than 1000 Hz, the coefficients of error function produced by the Mexican hat wavelet are smaller than the corresponding values of the Morlet and Meyer wavelets. It means that the Mexican hat wavelet has higher degree of similarity to the impulse noise signal than the Morlet and Meyer wavelets at small scales. Comparatively, when the scales are larger than 40, the Morlet and Mayer wavelets have higher similarity to the impulse noise signal than the Mexican hat wavelet. The results indicate that the Mexican can represent much superior features of the A-wave impulse noise signals at higher frequency range, which responses to the short time duration such as A-duration $t+$ shown in Fig. 4c. While the Morlet and Meyer wavelets may perform better when representing lower frequency components in an impulse noise signal, such as the time duration of negative pressure $t-$ shown in Fig. 4c.

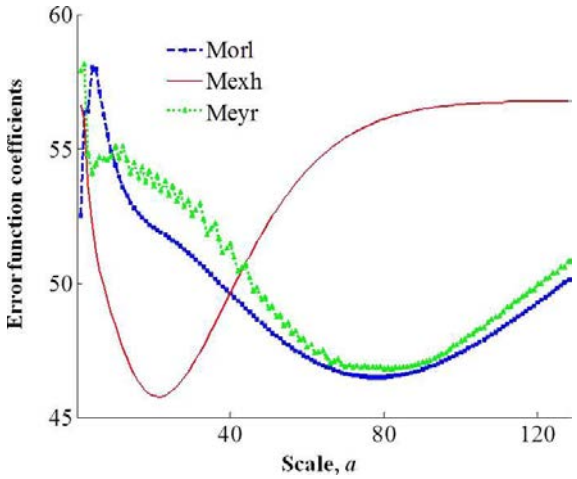

Fig. 11. The similarities between the impulse noise signal and three wavelet functions under different scales. The similarities are inversely presented by the error function coefficients.

5. Conclusion

In this paper, we applied CWT for the analysis of A-wave impulse noise, and compared the performances of three different wavelets (i.e., Morlet, Mexican hat, and Meyer wavelets). All three wavelets can represent detailed features of the impulse noise in the T-F domain. The Mexican hat wavelet shows advantages over the Morlet and Meyer wavelets for impulse

noise analysis. The Mexican hat wavelet also shows the lowest wavelet entropy level and highest degree of the similarity to the signal of impulse noise among three wavelets. The results of wavelet entropy and similarity may explain why the Mexican hat wavelet can represent superior features of the impulse noise signals compared with the other two wavelets. The results of this study provide useful information for applying wavelet transform on analysis of A-wave impulse noise signals, and accordingly improve understanding of A-wave impulse noise induced hearing loss. However, other types of impulse noise, such as impact noise (Henderson, Hamernik, 1986) and alpha-stable impulsive noise (Ilow, Hatzinakos, 1998) are not included in this wavelet analysis framework. Further study will be done to apply CWT for analysis and characterization of different types of noises, including continuous noise, impulse noise, and complex noise.

Acknowledgment

This research was supported in part by the US Department of Defense (DoD) through grant number: W81XWH-11-C-0033.

References

1. Adeli H., Zhou Z., Dadmehr N. (2003), *Analysis of EEG records in an epileptic patient using wavelet transform*, Journal of Neuroscience Methods, **123**, 1, 69–87.
2. Agrawal Y., Platz E., Niparko J.K. (2008), *Prevalence of hearing loss and differences by demographic characteristics among US adults: data from the National Health and Nutrition Examination Survey, 1999–2004*, Arch. Intern. Med., **168**, 14, 1522–1530.
3. Chapa J.O., Rao R.M. (2000), *Algorithms for designing wavelets to match a specified signal*, IEEE Transactions on Signal Processing, **48**, 12, 3395–3406.
4. Clifford R.E., Rogers R.A. (2009), *Impulse noise: theoretical solutions to the quandary of cochlear protection*, Annals of Otology Rhinology and Laryngology, **118**, 6, 417–427.
5. Coifman R.R., Wickerhauser M.V. (1992), *Entropy-based algorithms for best basis selection*, IEEE Transactions on Information Theory, **38**, 2, 713–718.
6. Daubechies I. (1992), *Ten Lectures on Wavelets*, SIAM, Philadelphia.
7. Hamernik R.P., Ahroon W.A., Hsueh K.D., Lei S.F., Davis R.I. (1993), *Audiometric and histological differences between the effects of continuous and impulsive noise exposures*, Journal of the Acoustical Society of America, **93**, 4, 2088–2095.
8. Henderson D., Hamernik R.P. (1986), *Impulse noise – critical review*, Journal of the Acoustical Society of America, **80**, 2, 569–584.
9. Kim J., Welcome D.E., Dong R.G., Song W.J., Hayden C. (2007), *Time-frequency characterization of hand-transmitted, impulsive vibrations using analytic wavelet transform*, Journal of Sound and Vibration, **308**, 1, 98–111.
10. Ilow J., Hatzinakos D. (1998), *Analytic alpha-stable noise modeling in a Poisson field of interferers or scatterers*, Signal Processing, IEEE Transactions on, **46**, 6, 1601–1611.
11. Lin J., Qu L.S. (2000), *Feature extraction based on Morlet wavelet and its application for mechanical fault diagnosis*, Journal of Sound and Vibration, **234**, 1, 135–148.
12. Mallat S. (1997), *A wavelet Tour of Signal Processing*, Academic Press, New York.
13. Price G.R., Kim H.N., Lim D.J., Dunn D. (1989), *Hazard from weapons impulses – histological and electrophysiological evidence*, Journal of the Acoustical Society of America **85**, 3, 1245–1254.
14. Rosso O.A., Blanco S., Yordanova J., Kolev V., Figliola A., Schurmann M., Basar E. (2001), *Wavelet entropy: a new tool for analysis of short duration brain electrical signals*, Journal of Neuroscience Methods, **105**, 1, 65–75.
15. Satish L., Nazneen B. (2003), *Wavelet-based denoising of partial discharge signals buried in excessive noise and interference*, IEEE Transactions on Dielectrics and Electrical Insulation, **10**, 2, 354–367.
16. Senhadji L., Wendling F. (2002), *Epileptic transient detection: wavelets and time-frequency approaches*, Neurophysiologie Clinique-Clinical Neurophysiology, **32**, 3, 175–192.
17. Smith G. (1996), *Noise? What noise?*, Occupational Health & Safety, **65**, 3, 38.
18. Wang W.J., McFadden P.D. (1996), *Application of wavelets to gearbox vibration signals for fault detection*, Journal of Sound and Vibration, **192**, 5, 927–939.
19. Wu Q., Qin J. (2013), *Effects of key parameters of impulse noise on prediction of the auditory hazard using AHAAH model*, International Journal of Computational Biology and Drug Design, **6**, 3, 210–220.
20. Young R.K. (1993), *Wavelet theory and its applications*, Springer, New York.
21. Zhu X.D., Kim J. (2006), *Application of analytic wavelet transform to analysis of highly impulsive noises*, Journal of Sound and Vibration, **294**, 4, 841–855.